EUROPEAN LABORATORY FOR PARTICLE PHYSICS

CERN-EP/98-106
3 July 1998

Production of χ_{c2} Mesons in Photon-Photon Collisions at LEP

The OPAL Collaboration

Abstract

We present an observation at LEP of the production of χ_{c2} mesons in the collisions of two quasi-real photons using the OPAL detector. The χ_{c2} mesons are reconstructed in the decay channel $\chi_{c2} \to J/\psi\ \gamma \to \ell^+\ \ell^-\ \gamma$ (with $\ell = e, \mu$) using all data taken at e^+e^- centre-of-mass energies of 91 and 183 GeV, corresponding to integrated luminosities of 167 and 55 pb^{-1} respectively. The two-photon width of the χ_{c2} is determined to be

$$\Gamma(\chi_{c2} \to \gamma\gamma) = 1.76 \pm 0.47 \pm 0.37 \pm 0.15 \text{ keV},$$

where the first error is statistical, the second is systematic and the third comes from branching ratio uncertainties.

(To be submitted to Physics Letters)

The OPAL Collaboration

K. Ackerstaff[8], G. Alexander[23], J. Allison[16], N. Altekamp[5], K.J. Anderson[9], S. Anderson[12], S. Arcelli[2], S. Asai[24], S.F. Ashby[1], D. Axen[29], G. Azuelos[18,a], A.H. Ball[17], E. Barberio[8], R.J. Barlow[16], R. Bartoldus[3], J.R. Batley[5], S. Baumann[3], J. Bechtluft[14], T. Behnke[27], K.W. Bell[20], G. Bella[23], A. Bellerive[9], S. Bentvelsen[8], S. Bethke[14], S. Betts[15], O. Biebel[14], A. Biguzzi[5], S.D. Bird[16], V. Blobel[27], I.J. Bloodworth[1], M. Bobinski[10], P. Bock[11], J. Böhme[14], M. Boutemeur[34], S. Braibant[8], P. Bright-Thomas[1], R.M. Brown[20], H.J. Burckhart[8], C. Burgard[8], R. Bürgin[10], P. Capiluppi[2], R.K. Carnegie[6], A.A. Carter[13], J.R. Carter[5], C.Y. Chang[17], D.G. Charlton[1,b], D. Chrisman[4], C. Ciocca[2], P.E.L. Clarke[15], E. Clay[15], I. Cohen[23], J.E. Conboy[15], O.C. Cooke[8], C. Couyoumtzelis[13], R.L. Coxe[9], M. Cuffiani[2], S. Dado[22], G.M. Dallavalle[2], R. Davis[30], S. De Jong[12], L.A. del Pozo[4], A. de Roeck[8], K. Desch[8], B. Dienes[33,d], M.S. Dixit[7], J. Dubbert[34], E. Duchovni[26], G. Duckeck[34], I.P. Duerdoth[16], D. Eatough[16], P.G. Estabrooks[6], E. Etzion[23], H.G. Evans[9], F. Fabbri[2], A. Fanfani[2], M. Fanti[2], A.A. Faust[30], F. Fiedler[27], M. Fierro[2], I. Fleck[8], R. Folman[26], A. Fürtjes[8], D.I. Futyan[16], P. Gagnon[7], J.W. Gary[4], J. Gascon[18], S.M. Gascon-Shotkin[17], G. Gaycken[27], C. Geich-Gimbel[3], G. Giacomelli[2], P. Giacomelli[2], V. Gibson[5], W.R. Gibson[13], D.M. Gingrich[30,a], D. Glenzinski[9], J. Goldberg[22], W. Gorn[4], C. Grandi[2], E. Gross[26], J. Grunhaus[23], M. Gruwé[27], G.G. Hanson[12], M. Hansroul[8], M. Hapke[13], K. Harder[27], C.K. Hargrove[7], C. Hartmann[3], M. Hauschild[8], C.M. Hawkes[5], R. Hawkings[27], R.J. Hemingway[6], M. Herndon[17], G. Herten[10], R.D. Heuer[8], M.D. Hildreth[8], J.C. Hill[5], S.J. Hillier[1], P.R. Hobson[25], A. Hocker[9], R.J. Homer[1], A.K. Honma[28,a], D. Horváth[32,c], K.R. Hossain[30], R. Howard[29], P. Hüntemeyer[27], P. Igo-Kemenes[11], D.C. Imrie[25], K. Ishii[24], F.R. Jacob[20], A. Jawahery[17], H. Jeremie[18], M. Jimack[1], C.R. Jones[5], P. Jovanovic[1], T.R. Junk[6], D. Karlen[6], V. Kartvelishvili[16], K. Kawagoe[24], T. Kawamoto[24], P.I. Kayal[30], R.K. Keeler[28], R.G. Kellogg[17], B.W. Kennedy[20], A. Klier[26], S. Kluth[8], T. Kobayashi[24], M. Kobel[3,e], D.S. Koetke[6], T.P. Kokott[3], M. Kolrep[10], S. Komamiya[24], R.V. Kowalewski[28], T. Kress[11], P. Krieger[6], J. von Krogh[11], T. Kuhl[3], P. Kyberd[13], G.D. Lafferty[16], D. Lanske[14], J. Lauber[15], S.R. Lautenschlager[31], I. Lawson[28], J.G. Layter[4], D. Lazic[22], A.M. Lee[31], D. Lellouch[26], J. Letts[12], L. Levinson[26], R. Liebisch[11], B. List[8], C. Littlewood[5], A.W. Lloyd[1], S.L. Lloyd[13], F.K. Loebinger[16], G.D. Long[28], M.J. Losty[7], J. Ludwig[10], D. Liu[12], A. Macchiolo[2], A. Macpherson[30], W. Mader[3], M. Mannelli[8], S. Marcellini[2], C. Markopoulos[13], A.J. Martin[13], J.P. Martin[18], G. Martinez[17], T. Mashimo[24], P. Mättig[26], W.J. McDonald[30], J. McKenna[29], E.A. Mckigney[15], T.J. McMahon[1], R.A. McPherson[28], F. Meijers[8], S. Menke[3], F.S. Merritt[9], H. Mes[7], J. Meyer[27], A. Michelini[2], S. Mihara[24], G. Mikenberg[26], D.J. Miller[15], R. Mir[26], W. Mohr[10], A. Montanari[2], T. Mori[24], K. Nagai[8], I. Nakamura[24], H.A. Neal[12], B. Nellen[3], R. Nisius[8], S.W. O'Neale[1], F.G. Oakham[7], F. Odorici[2], H.O. Ogren[12], M.J. Oreglia[9], S. Orito[24], J. Pálinkás[33,d], G. Pásztor[32], J.R. Pater[16], G.N. Patrick[20], J. Patt[10], R. Perez-Ochoa[8], S. Petzold[27], P. Pfeifenschneider[14], J.E. Pilcher[9], J. Pinfold[30], D.E. Plane[8], P. Poffenberger[28], B. Poli[2], J. Polok[8], M. Przybycień[8], C. Rembser[8], H. Rick[8], S. Robertson[28], S.A. Robins[22], N. Rodning[30], J.M. Roney[28], K. Roscoe[16], A.M. Rossi[2], Y. Rozen[22], K. Runge[10], O. Runolfsson[8], D.R. Rust[12], K. Sachs[10], T. Saeki[24], O. Sahr[34], W.M. Sang[25], E.K.G. Sarkisyan[23], C. Sbarra[29], A.D. Schaile[34], O. Schaile[34], F. Scharf[3], P. Scharff-Hansen[8], J. Schieck[11], B. Schmitt[8], S. Schmitt[11], A. Schöning[8], M. Schröder[8], M. Schumacher[3], C. Schwick[8], W.G. Scott[20], R. Seuster[14], T.G. Shears[8], B.C. Shen[4], C.H. Shepherd-Themistocleous[8], P. Sherwood[15], G.P. Siroli[2], A. Sittler[27], A. Skuja[17], A.M. Smith[8], G.A. Snow[17], R. Sobie[28], S. Söldner-Rembold[10], M. Sproston[20], A. Stahl[3], K. Stephens[16], J. Steuerer[27], K. Stoll[10], D. Strom[19], R. Ströhmer[34], B. Surrow[8], S.D. Talbot[1],

S. Tanaka[24], P. Taras[18], S. Tarem[22], R. Teuscher[8], M. Thiergen[10], M.A. Thomson[8], E. von Törne[3], E. Torrence[8], S. Towers[6], I. Trigger[18], Z. Trócsányi[33], E. Tsur[23], A.S. Turcot[9], M.F. Turner-Watson[8], R. Van Kooten[12], P. Vannerem[10], M. Verzocchi[10], H. Voss[3], F. Wäckerle[10], A. Wagner[27], C.P. Ward[5], D.R. Ward[5], P.M. Watkins[1], A.T. Watson[1], N.K. Watson[1], P.S. Wells[8], N. Wermes[3], J.S. White[6], G.W. Wilson[16], J.A. Wilson[1], T.R. Wyatt[16], S. Yamashita[24], G. Yekutieli[26], V. Zacek[18], D. Zer-Zion[8]

[1]School of Physics and Astronomy, University of Birmingham, Birmingham B15 2TT, UK
[2]Dipartimento di Fisica dell' Università di Bologna and INFN, I-40126 Bologna, Italy
[3]Physikalisches Institut, Universität Bonn, D-53115 Bonn, Germany
[4]Department of Physics, University of California, Riverside CA 92521, USA
[5]Cavendish Laboratory, Cambridge CB3 0HE, UK
[6]Ottawa-Carleton Institute for Physics, Department of Physics, Carleton University, Ottawa, Ontario K1S 5B6, Canada
[7]Centre for Research in Particle Physics, Carleton University, Ottawa, Ontario K1S 5B6, Canada
[8]CERN, European Organisation for Particle Physics, CH-1211 Geneva 23, Switzerland
[9]Enrico Fermi Institute and Department of Physics, University of Chicago, Chicago IL 60637, USA
[10]Fakultät für Physik, Albert Ludwigs Universität, D-79104 Freiburg, Germany
[11]Physikalisches Institut, Universität Heidelberg, D-69120 Heidelberg, Germany
[12]Indiana University, Department of Physics, Swain Hall West 117, Bloomington IN 47405, USA
[13]Queen Mary and Westfield College, University of London, London E1 4NS, UK
[14]Technische Hochschule Aachen, III Physikalisches Institut, Sommerfeldstrasse 26-28, D-52056 Aachen, Germany
[15]University College London, London WC1E 6BT, UK
[16]Department of Physics, Schuster Laboratory, The University, Manchester M13 9PL, UK
[17]Department of Physics, University of Maryland, College Park, MD 20742, USA
[18]Laboratoire de Physique Nucléaire, Université de Montréal, Montréal, Quebec H3C 3J7, Canada
[19]University of Oregon, Department of Physics, Eugene OR 97403, USA
[20]CLRC Rutherford Appleton Laboratory, Chilton, Didcot, Oxfordshire OX11 0QX, UK
[22]Department of Physics, Technion-Israel Institute of Technology, Haifa 32000, Israel
[23]Department of Physics and Astronomy, Tel Aviv University, Tel Aviv 69978, Israel
[24]International Centre for Elementary Particle Physics and Department of Physics, University of Tokyo, Tokyo 113, and Kobe University, Kobe 657, Japan
[25]Institute of Physical and Environmental Sciences, Brunel University, Uxbridge, Middlesex UB8 3PH, UK
[26]Particle Physics Department, Weizmann Institute of Science, Rehovot 76100, Israel
[27]Universität Hamburg/DESY, II Institut für Experimental Physik, Notkestrasse 85, D-22607 Hamburg, Germany
[28]University of Victoria, Department of Physics, P O Box 3055, Victoria BC V8W 3P6, Canada
[29]University of British Columbia, Department of Physics, Vancouver BC V6T 1Z1, Canada
[30]University of Alberta, Department of Physics, Edmonton AB T6G 2J1, Canada
[31]Duke University, Dept of Physics, Durham, NC 27708-0305, USA

[32]Research Institute for Particle and Nuclear Physics, H-1525 Budapest, P O Box 49, Hungary
[33]Institute of Nuclear Research, H-4001 Debrecen, P O Box 51, Hungary
[34]Ludwigs-Maximilians-Universität München, Sektion Physik, Am Coulombwall 1, D-85748 Garching, Germany

[a] and at TRIUMF, Vancouver, Canada V6T 2A3
[b] and Royal Society University Research Fellow
[c] and Institute of Nuclear Research, Debrecen, Hungary
[d] and Department of Experimental Physics, Lajos Kossuth University, Debrecen, Hungary
[e] on leave of absence from the University of Freiburg

1 Introduction

We present a LEP measurement of the two-photon width $\Gamma(\chi_{c2} \to \gamma\gamma)$ for the production of χ_{c2} mesons in photon-photon interactions. The χ_{c2} is observed through its decay to a J/ψ and a photon, with the J/ψ identified through its decay to e^+e^- or $\mu^+\mu^-$. All LEP1 and LEP2 data samples taken at centre-of-mass energies $\sqrt{s}_{ee}$ of 91 and 183 GeV are used, corresponding to integrated luminosities $L = 167$ and 55 pb^{-1}, respectively.

The χ_{c2} meson is a $c\bar{c}$ bound state with spin-parity $J^{PC} = 2^{++}$ which can therefore be produced in the collision of two photons. At LEP, virtual photons (denoted by γ^*) are emitted by the beam electrons[1]. The χ_{c2} mesons can therefore be produced in the process $e^+e^- \to e^+e^-\gamma^*\gamma^* \to e^+e^-\chi_{c2}$. Since the photons carry only small negative squared four-momenta Q^2, they are assumed to be quasi-real ($Q^2 \approx 0$).

The two-photon width $\Gamma_{\gamma\gamma}$ measures the coupling of two real photons to a resonance and is directly proportional to the production cross-section in $\gamma\gamma$ collisions. Due to the relatively large mass m_c of the c quarks the χ_{c2} meson can be treated non-relativistically and perturbatively. The ratio of the widths of the χ_{c2} decaying to two photons and to two gluons can be directly related to the ratio of the electromagnetic and strong coupling constants:

$$\frac{\Gamma(\chi_{c2} \to \gamma\gamma)}{\Gamma(\chi_{c2} \to gg)} = \frac{8}{9}\left(\frac{\alpha_{em}}{\alpha_s(m_c)}\right)^2. \quad (1)$$

In simple models $\Gamma(\chi_{c2} \to gg) \approx \Gamma(\chi_{c2} \to \text{hadrons})$. Using $\Gamma(\chi_{c2} \to \text{hadrons})$ measured in $p\overline{p}$ scattering [1] and $\alpha_s(m_c) = 0.3$, we expect $\Gamma(\chi_{c2} \to \gamma\gamma)$ to be of the order of 1 keV. Based on a QCD model of Bodwin et al. [2] a value of $\Gamma(\chi_{c2} \to \gamma\gamma) = 0.82 \pm 0.30$ keV is obtained. A recent calculation by Schuler [3] predicts a smaller value for $\Gamma(\chi_{c2} \to \gamma\gamma)$ of 0.28 keV. The experimental results on the two-photon width $\Gamma(\chi_{c2} \to \gamma\gamma)$ measured in e^+e^- [4, 5] and $p\overline{p}$ collisions [6, 7] are summarised in Table 1. The measurements vary over an order of magnitude. The result 0.321 ± 0.095 keV, obtained by E760 [6] from the process $p\overline{p} \to \chi_{c2} \to \gamma\gamma$, dominates the current world average of 0.37 ± 0.17 keV [8].

[1]Positrons are also referred to as electrons

2 The OPAL detector

A detailed description of the OPAL detector can be found in Ref. [9], and therefore only a brief account of the main features relevant to the present analysis will be given here.

The central tracking system is located inside a solenoidal magnet which provides a uniform axial magnetic field of 0.435 T along the beam axis[2]. The detection efficiency for charged particles is close to 100 % within the polar angle range $|\cos\theta| < 0.92$. The magnet is surrounded in the barrel region ($|\cos\theta| < 0.82$) by a lead glass electromagnetic calorimeter (ECAL) and a hadronic sampling calorimeter (HCAL). Outside the HCAL, the detector is surrounded by muon chambers. There are similar layers of detectors in the endcaps ($0.81 < |\cos\theta| < 0.98$). The small angle region from 47 to 140 mrad around the beam pipe on both sides of the interaction point is covered by the forward calorimeters (FD) and the region from 25 to 59 mrad by the silicon tungsten luminometers (SW). From 1996 onwards, which includes the data-taking period at $\sqrt{s}_{\mathrm{ee}} = 183$ GeV presented in this paper, the lower boundary of the acceptance has been increased to 33 mrad following the installation of a low angle shield to protect the central detector against possible synchrotron radiation.

Starting with the innermost components, the tracking system consists of a high precision silicon microvertex detector, a vertex drift chamber, a large-volume jet chamber with 159 layers of axial anode wires and a set of z chambers measuring the track coordinates along the beam direction. The transverse momenta p_{T} of tracks with respect to the z axis are measured with a precision parametrised by $\sigma_{p_{\mathrm{T}}}/p_{\mathrm{T}} = \sqrt{0.02^2 + (0.0015 \cdot p_{\mathrm{T}})^2}$ (p_{T} in GeV/c) in the central region. The jet chamber also provides measurements of the energy loss, $\mathrm{d}E/\mathrm{d}x$, which are used for particle identification [9].

The barrel and endcap sections of the ECAL are both constructed from lead glass blocks with a depth of 24.6 radiation lengths in the barrel region and more than 22 radiation lengths in the endcaps. The FD consist of cylindrical lead-scintillator calorimeters with a depth of 24 radiation lengths divided azimuthally into 16 segments. The electromagnetic energy resolution is about $18\%/\sqrt{E}$, where E is in GeV. The SW detectors [10] consist of 19 layers of silicon and 18 layers of tungsten, corresponding to a total of 22 radiation lengths. Each silicon layer consists of 16 wedge shaped silicon detectors. The electromagnetic energy resolution is about $25\%/\sqrt{E}$ (E in GeV).

3 Process kinematics and Monte Carlo simulation

The $\mathrm{e^+e^-}$ cross-section for the production of χ_{c2} mesons in two-photon events can be described by the product of the $\gamma\gamma$ luminosity function $\mathcal{L}_{\gamma\gamma}$ and the cross-section σ of the process $\gamma^*\gamma^* \to \chi_{\mathrm{c2}}$:

$$\sigma(\mathrm{e^+e^-} \to \mathrm{e^+e^-}\chi_{\mathrm{c2}}) = \mathcal{L}_{\gamma\gamma}(\mathrm{e^+e^-} \to \mathrm{e^+e^-}\gamma^*\gamma^*)\sigma(\gamma^*\gamma^* \to \chi_{\mathrm{c2}}). \quad (2)$$

Since most photons have a small negative squared four-momentum-transfer Q^2, the photons are considered to be quasi-real with helicity ± 1, i.e. they are transverse. Thus only the luminosity

[2] In the OPAL coordinate system the z axis points in the direction of the $\mathrm{e^-}$ beam. The polar angle θ, the azimuthal angle ϕ and the radius r denote the usual spherical coordinates.

function describing two transverse photons contributes. The two-photon formation cross-section for the χ_{c2} resonance with this assumption [11] is

$$\sigma(\gamma^*\gamma^* \to \chi_{c2}) = 8\pi(2J_{\chi_{c2}}+1)\Gamma(\chi_{c2}\to\gamma\gamma)\frac{\Gamma_{\rm tot}}{(W^2-M^2_{\chi_{c2}})^2+M^2_{\chi_{c2}}\Gamma^2_{\rm tot}}, \tag{3}$$

where $J_{\chi_{c2}}$ denotes the spin of the χ_{c2}, $M_{\chi_{c2}}$ its mass, $\Gamma_{\rm tot}$ its total width and W the invariant mass of the two-photon system. The total cross-section for the process $e^+e^- \to e^+e^-\chi_{c2}$ can be written as [11]:

$$\sigma(e^+e^- \to e^+e^-\chi_{c2}) = (2J_{\chi_{c2}}+1)\frac{8\alpha^2_{\rm em}\Gamma(\chi_{c2}\to\gamma\gamma)}{M^3_{\chi_{c2}}}g(M^2_{\chi_{c2}}/s_{ee}), \tag{4}$$

where the dependence on the squared e^+e^- centre-of-mass energy s_{ee} is contained in the function

$$g(z) = \left(\left(1+\frac{1}{2}z\right)^2\ln\frac{1}{z} - \frac{1}{2}(1-z)(3+z)\right)\left(\ln\frac{M^2_{J/\psi}}{zM^2_e}-1\right)^2 - \frac{1}{3}\left(\ln\frac{1}{z}\right)^3. \tag{5}$$

This expression is obtained by integrating the luminosity function based on the equivalent photon approximation (EPA). Further parameters are the electron mass M_e and the mass $M_{J/\psi}$ of the J/ψ meson that enters into the form factor. By measuring $\sigma(e^+e^- \to e^+e^-\chi_{c2})$ the two-photon width $\Gamma(\chi_{c2}\to\gamma\gamma)$ can be calculated.

The Monte Carlo Generator TWOGEN [12] is used to generate the process $\gamma^*\gamma^* \to \chi_{c2}$ according to Eq. 3. The decay of the resonance is handled by JETSET 7.408 [13] taking into account final state radiation of the two decay leptons. The polar angles of the scattered electrons in the process $e^+e^- \to e^+e^-\gamma^*\gamma^*$ are allowed to vary from 0 to π. The Q^2 dependence of the χ_{c2} production cross-section is modelled with a J/ψ form factor. All Monte Carlo events were generated with a full simulation of the OPAL detector [14].

Only helicity ±2 is relevant for the χ_{c2} production amplitude [15] where the helicity is defined with respect to the χ_{c2} direction of motion in the laboratory system which is collinear with the axis of the incoming photons. In the decay of the χ_{c2} the photon carries an angular momentum of 1, 2 or 3 (in units of $\hbar$). Since the χ_{c2} and the J/ψ have opposite parity, electric dipole (E1), magnetic quadrupole (M2) and electric octupole (E3) transitions are possible. In terms of helicities, decay amplitudes for helicity 0, ±1 and ±2 parametrise the dynamics of the χ_{c2} decay process. These decay helicity amplitudes are defined with respect to the J/ψ γ axis and are related to the angular momentum carried by the photon.

Three angles are necessary to describe the χ_{c2} decay to a J/ψ and a γ with the subsequent decay of the J/ψ to a lepton pair. These angles are illustrated in Fig. 1. The polar angle θ^* is measured in the χ_{c2} rest frame and is the angle between the χ_{c2} direction of motion in the laboratory system and the outgoing decay photon. The polar and azimuthal angles of the positive decay lepton, θ' and ϕ', are measured in the J/ψ rest frame with the z' axis given by the direction opposite to the photon's direction from the χ_{c2} decay, and the x' axis in the plane containing the χ_{c2} direction and the incident photons.

In TWOGEN the events are generated flat in $\cos\theta^*$, $\cos\theta'$ and ϕ'. The Monte Carlo events are re-weighted according to the appropriate angular distribution of the $\chi_{c2} \to J/\psi\ \gamma$ decay.

The full expression for the angular distribution is given in the Appendix. All decay amplitudes for helicities 0, ± 1 and ± 2 are taken into account.

We also used the Monte Carlo generator GALUGA [16] to generate χ_{c2} events. The selection efficiency for χ_{c2} events is found to be consistent with the selection efficiency determined with TWOGEN. In addition, GALUGA is used to generate the possible resonant background process $e^+e^- \to e^+e^-\chi_{c1}$.

4 Event selection

The production of χ_{c2} mesons in two-photon events is studied using the data taken at centre-of-mass energies $\sqrt{s}_{ee}$ of 91 and 183 GeV. The same set of cuts for both centre-of-mass energies is applied to the data to select χ_{c2} candidate events:

- The sum of all energy deposits has to be less than 30 GeV in the ECAL and less than 20 GeV in the HCAL. These cuts mainly reject two-fermion events.
- Tracks are required to have at least 20 hits in the central jet chamber used for the determination of the specific energy loss $\mathrm{d}E/\mathrm{d}x$. Events are required to contain exactly two oppositely charged tracks, where the two tracks must have a minimum transverse momentum p_T with respect to the z axis of the detector of 800 MeV/c. This reduces the background from leptonic two-photon events with a small invariant mass W. The distance of the point of closest approach to the origin of the tracks in the $r\phi$ plane must be less than 5 cm in the z direction and less than 1 cm in the $r\phi$ plane. The invariant mass of the two tracks must lie in the range between 2.7 and 3.5 GeV/c^2, close to the mass of the J/ψ. In order to ensure that the final state consists of only two tracks, no additional track with $p_T > 120$ MeV/c and more than 20 $\mathrm{d}E/\mathrm{d}x$ hits is allowed.
- After these cuts the main background contribution is expected to be leptonic two-photon events, $e^+e^- \to e^+e^-e^+e^-$ and $e^+e^- \to e^+e^-\mu^+\mu^-$. To reduce this background, the transverse momentum with respect to the z axis, $p_T^{J/\psi}$, of the J/ψ candidate formed by the two tracks is required to be larger than 100 MeV/c.
- For the case where the J/ψ decays to a muon (electron) pair, the two tracks are identified as muons (electrons) if the $\mathrm{d}E/\mathrm{d}x$ probability for the muon (electron) hypothesis exceeds 1%.
- The event is rejected if a cluster with an energy deposit larger than 1 GeV is observed in the FD or SW.
- There must be exactly one photon candidate in an event. A cluster in the ECAL is treated as a photon candidate if it fulfils the following requirements:
  - The measured cluster energy, E_γ^{meas}, should be at least 300 MeV. In order to reduce background from ECAL clusters in the regions close to the beam pipe and in the overlap regions between the endcaps and the barrel, clusters with $|\cos\theta_\gamma| > 0.96$ and clusters with $0.84 < |\cos\theta_\gamma| < 0.85$ are not considered where θ_γ is the polar angle of the cluster with respect to the z axis.

  - The angles between the cluster and each track momentum should exceed 300 mrad to reject events with final-state radiation in leptonic two-photon events.

- The angle in the $r\phi$ plane between the photon and the J/ψ candidate formed by the two tracks must be greater than 150°.

After these preselection cuts, 203 events remain at $\sqrt{s}_{\mathrm{ee}} = 91$ GeV and 53 events at $\sqrt{s}_{\mathrm{ee}} = 183$ GeV.

5 χ_{c2} reconstruction and results

For signal events, the photon is one of the decay particles in a two-body decay, and so its energy is kinematically fixed to be 430 MeV in the χ_{c2} rest frame. Due to the Lorentz boost of the $\gamma\gamma$ system, the energy of most photons is higher in the laboratory system but still often below 1 GeV. In Figure 2a, the difference between the generated and the measured photon energy after the detector response, $E_\gamma^{\mathrm{gen}} - E_\gamma^{\mathrm{meas}}$, is shown for Monte Carlo events after applying the cuts described in Section 4. In this regime the energy resolution of the ECAL does not allow a sufficiently precise measurement of the photon energy.

From momentum conservation, the transverse momentum of the photon is balanced by the transverse momentum sum $p_{\mathrm{T}}^{\mathrm{J}/\psi}$ of the two tracks. For the signal photon candidates, the energy and momentum is therefore reconstructed using the relation

$$E_\gamma^{\mathrm{rec}} = \frac{p_{\mathrm{T}}^{\mathrm{J}/\psi}}{\sin\theta_\gamma}, \tag{6}$$

with θ_γ being the polar angle of the ECAL cluster assumed to originate from the photon. This procedure improves the energy resolution significantly. The distribution of the difference between the generated and the reconstructed photon energy, $E_\gamma^{\mathrm{gen}} - E_\gamma^{\mathrm{rec}}$, is significantly narrower (Figure 2b).

Figure 3 shows the invariant mass spectrum of the two tracks after applying all cuts and after requiring the invariant mass of the lepton-lepton-photon ($\ell\ell\gamma$) system to lie in the range $3.40 < M_{\ell\ell\gamma} < 3.65$ GeV/c^2 around $M_{\chi_{c2}}$. The invariant mass $M_{\ell\ell\gamma}$ of the $\ell\ell\gamma$ system is calculated using the photon energy E_γ^{rec} reconstructed via Eq. 6. A significant peak is visible around the mass of the J/ψ at 3.1 GeV/c^2. The Monte Carlo simulation, represented by the histogram, shows a small tail towards lower invariant masses. This is due to bremsstrahlung and final state radiation of the leptons.

For a χ_{c2} event the invariant mass of the two tracks must be the mass of the J/ψ. Therefore a constrained fit is performed using a program by Blobel [17]. For each track, the curvature, the azimuthal angle, the polar angle in the form $\cot\theta$ and the complete covariance matrix are used in the fitting algorithm. From the fit we obtain a χ^2 probability $\mathcal{P}(J/\psi)$ for the J/ψ hypothesis.

The mass difference between the $\ell\ell\gamma$ and the $\ell\ell$ system, $M_{\ell\ell\gamma} - M_{\ell\ell}$, is used to study the χ_{c2} signal. This minimizes effects from the broadening of the $\ell\ell\gamma$ and the $\ell\ell$ mass spectrum due to

final state radiation of the leptons. The distribution of the mass difference, $M_{\ell\ell\gamma} - M_{\ell\ell}$, is shown in Fig. 4 for $\mathcal{P}(J/\psi) > 1\%$. A significant peak shows up around $M_{\ell\ell\gamma} - M_{\ell\ell} = 459$ MeV/c^2 with $N^{\rm SEL}_{\ell\ell\gamma} = 34$ events counted in the signal region between $330 < M_{\ell\ell\gamma} - M_{\ell\ell} < 580$ MeV/c^2. The two tracks are identified as electrons in 11 of the 34 selected events and in 23 events as muons. This is consistent with the ratio of the Monte Carlo selection efficiencies for J/ψ decays to electrons and muons, respectively. Furthermore, 7 of the 34 events are selected at $\sqrt{s}_{\rm ee} = 183$ GeV which is consistent with the ratio of $\chi_{\rm c2}$ events expected for the two $\rm e^+e^-$ centre-of-mass energies. Fitting a Gaussian with a power tail plus a linear background function to the data, where the exponent of the power tail was determined from the Monte Carlo, yields a mean value of $\langle M_{\ell\ell\gamma} - M_{\ell\ell}\rangle = 464 \pm 14$ MeV/c^2 and a width of 39 ± 16 MeV/c^2 compared to $\langle M_{\ell\ell\gamma} - M_{\ell\ell}\rangle = 459 \pm 1$ MeV/c^2 and a width of 37 ± 1 MeV/c^2 in the Monte Carlo.

The two-photon width $\Gamma(\chi_{\rm c2} \to \gamma\gamma)$ is calculated from the number of events in the signal region, $N^{\rm SEL}_{\ell\ell\gamma}$, and the number of background events in the signal region, $N^{\rm BG}_{\ell\ell\gamma}$, with

$$\Gamma(\chi_{\rm c2} \to \gamma\gamma) = \frac{1}{(2J_{\chi_{\rm c2}}+1)} \, \frac{M^3_{\chi_{\rm c2}}}{8\alpha^2_{\rm em}} \, \frac{1}{\mathrm{BR}(\chi_{\rm c2} \to J/\psi\ \gamma)} \, \frac{1}{\mathrm{BR}(J/\psi \to \ell^+\ell^-)} \, \frac{N^{\rm SEL}_{\ell\ell\gamma} - N^{\rm BG}_{\ell\ell\gamma}}{\sum g(z) L \epsilon_{\chi_{\rm c2}}}, \qquad (7)$$

where the sum runs over the two $\rm e^+e^-$ centre-of-mass energies $\sqrt{s}_{\rm ee}$. The function $g(z)$ is defined by Eq. 5. The total integrated luminosities for $\sqrt{s}_{\rm ee} = 91$ and 183 GeV are $L = 167$ pb^{-1} and 55 pb^{-1}. The selection efficiency is determined by dividing the sum of the weights of the selected Monte Carlo events by the sum of the weights of all generated events. The selection efficiencies $\epsilon_{\chi_{\rm c2}}$ are 7.0% for $\sqrt{s}_{\rm ee} = 91$ GeV and 5.7% for $\sqrt{s}_{\rm ee} = 183$ GeV. Signal losses at the trigger level are found to be negligible. The branching ratios are $\mathrm{BR}(\chi_{\rm c2} \to J/\psi\ \gamma) = 0.135 \pm 0.011$ and $\mathrm{BR}(J/\psi \to \ell^+\ell^-) = 0.1203 \pm 0.0027$ [8].

The behaviour of the background is studied using the complementary $M_{\ell\ell\gamma} - M_{\ell\ell}$ distribution with $\mathcal{P}(\mathrm{J}/\psi) < 1\%$. Its shape is well described by a linear function. A linear function is therefore fitted to the sidebands of the $M_{\ell\ell\gamma} - M_{\ell\ell}$ spectrum with $\mathcal{P}(J/\psi) > 1\%$ in Fig. 4. The sidebands are defined by $M_{\ell\ell\gamma} - M_{\ell\ell} < 280$ MeV/c^2 and $M_{\ell\ell\gamma} - M_{\ell\ell} > 630$ MeV/c^2. For the fit, a maximum likelihood method for Poisson-distributed data was used [8]. The fit, which is superimposed, yields $N^{\rm BG}_{\ell\ell\gamma} = 12.4 \pm 3.3$ background events in the signal region. The $\chi_{\rm c2}$ Monte Carlo signal is added to the fitted background after normalising it to the number of signal minus background events in the signal region, $N^{\rm SEL}_{\ell\ell\gamma} - N^{\rm BG}_{\ell\ell\gamma}$, of the data.

There could be a small contribution to the $\chi_{\rm c2}$ signal from $\rm e^+e^- \to e^+e^-\chi_{c0}$ and $\rm e^+e^- \to e^+e^-\chi_{c1}$ events with $\chi_{\rm c0}$ and $\chi_{\rm c1}$ also decaying to $J/\psi\ \gamma$. These possible contributions would increase the measured two-photon width $\Gamma(\chi_{\rm c2} \to \gamma\gamma)$ with respect to the actual width. The mass peak of the $\chi_{\rm c0}$ meson is expected to be at $M_{\ell\ell\gamma} - M_{\ell\ell} = 318.2 \pm 1.0$ MeV/c^2 compared to 459.2 ± 0.2 MeV/c^2 expected for the $\chi_{\rm c2}$ [8]. Fig. 4 shows no indication for such a peak within the statistical errors.

In principle, the contribution from $\chi_{\rm c0}$ decays could be estimated from the data by measuring the decay angular distribution. In Fig. 5 the distribution of the polar angle of the photon, $\cos\theta^*$, is shown. The Monte Carlo expectation for an isotropic decay ($J = 0$) and for a decay angle distribution as described in Section 3 for $J = 2$ are superimposed. The agreement between data and Monte Carlo is reasonable in both cases. Due to the small number of data events, no further conclusion can be drawn concerning the decay angular distribution.

The production cross-section of χ_{c0} mesons in two-photon events can be calculated with Eq. 4. The ratio of the number of selected χ_{c2} events, $N_{\chi_{c2}}$, to the number of selected χ_{c0} events, $N_{\chi_{c0}}$, is given by:

$$\frac{N_{\chi_{c2}}}{N_{\chi_{c0}}} = \frac{\sigma(e^+e^- \to e^+e^-\chi_{c2})}{\sigma(e^+e^- \to e^+e^-\chi_{c0})} \cdot \frac{\mathrm{BR}(\chi_{c2} \to \mathrm{J}/\psi\,\gamma)}{\mathrm{BR}(\chi_{c0} \to \mathrm{J}/\psi\,\gamma)} \cdot \frac{\epsilon_{\chi_{c2}}}{\epsilon_{\chi_{c0}}} \quad (8)$$

$$= \frac{2J_{\chi_{c2}}+1}{2J_{\chi_{c0}}+1} \cdot \left(\frac{M_{\chi_{c0}}}{M_{\chi_{c2}}}\right)^3 \cdot \frac{\Gamma(\chi_{c2} \to \gamma\gamma)}{\Gamma(\chi_{c0} \to \gamma\gamma)} \cdot \frac{\mathrm{BR}(\chi_{c2} \to \mathrm{J}/\psi\,\gamma)}{\mathrm{BR}(\chi_{c0} \to \mathrm{J}/\psi\,\gamma)} \cdot \frac{\epsilon_{\chi_{c2}}}{\epsilon_{\chi_{c0}}}. \quad (9)$$

The spin factor equals 5, the mass term is of the order one and the branching ratio $\mathrm{BR}(\chi_{c2} \to \mathrm{J}/\psi\,\gamma)$ is about 20 times larger than the branching ratio $\mathrm{BR}(\chi_{c0} \to \mathrm{J}/\psi\,\gamma) = 0.0066 \pm 0.0018$ [8]. The same set of cuts as for χ_{c2} was applied to Monte Carlo χ_{c0} events yielding a selection efficiency $\epsilon_{\chi_{c0}} = 2.8\%$ for $330 < M_{\ell\ell\gamma} - M_{\ell\ell} < 580$ MeV/c^2 at $\sqrt{s}_{ee} = 91$ GeV. The two-photon width for the χ_{c0} has been measured to be $\Gamma(\chi_{c0} \to \gamma\gamma) = 5.4 \pm 3.7$ keV [18]. With this value and our measurement of $\Gamma(\chi_{c2} \to \gamma\gamma)$, the background due to χ_{c0} events is estimated to be 1.3%. This contribution is therefore neglected.

The case of the χ_{c1} meson is more complicated, although the production of spin-1 particles in the collisions of real photons is not allowed due to the Landau-Yang theorem [19]. But since the incoming photons have $Q^2 > 0$, the production of χ_{c1} mesons is possible. The χ_{c1} meson can not be well distinguished experimentally from the χ_{c2}, since their masses are almost degenerate. For the χ_{c1} mesons, the nominal mass difference $M_{\ell\ell\gamma} - M_{\ell\ell}$ is 413.6 ± 0.2 MeV/c^2 [8]. The selection efficiency for χ_{c1} events is determined using GALUGA which takes into account the Q^2 dependence for a spin-1 resonance. The selection efficiency is found to be much smaller, $\epsilon_{\chi_{c1}} \approx 0.1\%$ at $\sqrt{s}_{ee} = 91$ GeV, than for χ_{c2} production, because the average Q^2 of the χ_{c1} events is much higher and the transverse momentum of the χ_{c1} decay particles is therefore not balanced in the detector. Most of the χ_{c1} events are rejected due to the requirements that there should be no energy deposit in the FD or SW and that the angle in the $r\phi$ plane between the photon and the J/ψ candidate must be greater than 150°. Using the ratio of cross-sections given by the model of Schuler [3] and Eq. 8 for χ_{c1} instead of χ_{c0} mesons with $\mathrm{BR}(\chi_{c1} \to J/\psi\,\gamma) = 0.273 \pm 0.016$ [8], the contribution from χ_{c1} events is estimated to be much smaller than 1%. Background from ψ' production in e^+e^- annihilation events has been estimated to be negligible.

Equation 7 yields a measured two-photon width of

$$\Gamma(\chi_{c2} \to \gamma\gamma) = 1.76 \pm 0.47 \pm 0.37 \pm 0.15 \text{ keV}.$$

The first error is statistical, the second is systematic and the last error is due to the uncertainty of the branching ratios in the decay $\chi_{c2} \to J/\psi\,\gamma \to \ell\ell\gamma$.

6 Systematic errors

The following systematic errors are taken into account:

- The selection efficiency depends on the χ_{c2} decay angular distribution used in the Monte Carlo generation. In addition to the decay angular distribution as described in Section 3 the Monte Carlo events are weighted according to a pure electromagnetic dipole angular distribution (E1). This leads to a decrease of the measured two-photon width $\Gamma(\chi_{c2} \to \gamma\gamma)$ by 6%.

- The dependence on the form factor is studied using a ρ form factor and a Q^2 independent form factor instead of the default J/ψ form factor. The selection efficiencies as well as the cross-sections calculated with Eq. 4 change, together contributing a 5% uncertainty to $\Gamma(\chi_{c2} \to \gamma\gamma)$.

- The error due to the cut on the $\mathrm{d}E/\mathrm{d}x$ probabilities for the muon and electron hypotheses is estimated to be 4%.

- The minimum cluster energy of 300 MeV required in the ECAL for a photon candidate is an additional source of a systematic uncertainty. The energy resolution is given by the width of the $E_\gamma^{\mathrm{rec}} - E_\gamma^{\mathrm{meas}}$ distribution of the ECAL energy. If the energy resolution of the Monte Carlo is better than the actual resolution in the experiment, the selection efficiency from the Monte Carlo would be overestimated. To study this effect we exploit the fact that the reconstructed photon energy E_γ^{rec} is approximately equal to the generated photon energy E_γ^{gen} for a χ_{c2} event. This is shown in Figure 2b. The difference of the reconstructed and the measured photon energy, $E_\gamma^{\mathrm{rec}} - E_\gamma^{\mathrm{meas}}$, is shown in Figure 6 for data and Monte Carlo after all selection cuts. A Gaussian is fitted to both spectra yielding -169 ± 42 MeV for the mean in the data and -173 ± 5 MeV for the mean in the Monte Carlo. The widths are 181 ± 34 MeV for the data and 183 ± 4 MeV for the Monte Carlo. Mean and width are consistent within the statistical errors of the fit.

  The measured energy in the Monte Carlo is smeared with a Gaussian distribution in such a way that the decreased resolution in the Monte Carlo is approximately equal to the data resolution plus its error. This increases the measured $\Gamma(\chi_{c2} \to \gamma\gamma)$ by 11%.

- The error on the number of background events determined from the fit of a linear function to the sidebands of the signal in the mass difference spectrum corresponds to an additional uncertainty on $\Gamma(\chi_{c2} \to \gamma\gamma)$ of 15%.

- The statistical error of the Monte Carlo selection efficiency is 2%.

The error of the luminosity measurement is negligible. The systematic errors due to the modelling of the energy resolution and due to the background description are determined using the data and therefore inevitably contain a considerable statistical component. A summary of the errors is given in Table 2. The errors are added quadratically yielding a total systematic error of 21%.

7 Conclusions

We have measured the two-photon width $\Gamma(\chi_{c2} \to \gamma\gamma)$ in the process $\mathrm{e^+e^-} \to \mathrm{e^+e^-}\chi_{c2}$, with the χ_{c2} mesons reconstructed in the decay channel $\chi_{c2} \to J/\psi\ \gamma \to \ell^+\ \ell^-\ \gamma$ (with $\ell = e, \mu$).

The whole OPAL data samples taken at $\sqrt{s}_{\rm ee}$ of 91 and 183 GeV are used, corresponding to $L = 167$ pb^{-1} and 55 pb^{-1}. In total we have selected 34 events in the $\chi_{\rm c2}$ signal region $330 < M_{\ell\ell\gamma} - M_{\ell\ell} < 580$ MeV/c^2 including a background of 12.4 ± 3.3 events. The contribution from $\chi_{\rm c0}$ and $\chi_{\rm c1}$ events is estimated not to exceed a few percent. The two-photon width $\Gamma(\chi_{\rm c2} \to \gamma\gamma)$ is determined to be

$$\Gamma(\chi_{\rm c2} \to \gamma\gamma) = 1.76 \pm 0.47 \pm 0.37 \pm 0.15 \text{ keV}.$$

The first error is statistical, the second is systematic and the last error is due to the uncertainty of the branching ratios in the decay $\chi_{\rm c2} \to J/\psi\ \gamma \to \ell\ell\gamma$. In Table 1, a comparison of different measurements of the two-photon width $\Gamma(\chi_{\rm c2} \to \gamma\gamma)$ is given. Our result agrees with the results from CLEO, TPC/2γ and R704 if one takes into account the large statistical and systematic errors. Our result is about two standard deviations larger than the E760 result and the current world average [8] which is dominated by the E760 measurement. It is also more than two standard deviations larger than the prediction of Schuler [3].

Acknowledgements

We thank Michael Sivertz for providing the calculation of the decay angular distribution used by CLEO and Gerhard Schuler for useful discussions. We particularly wish to thank the SL Division for the efficient operation of the LEP accelerator at all energies and for their continuing close cooperation with our experimental group. We thank our colleagues from CEA, DAPNIA/SPP, CE-Saclay for their efforts over the years on the time-of-flight and trigger systems which we continue to use. In addition to the support staff at our own institutions we are pleased to acknowledge the
Department of Energy, USA,
National Science Foundation, USA,
Particle Physics and Astronomy Research Council, UK,
Natural Sciences and Engineering Research Council, Canada,
Israel Science Foundation, administered by the Israel Academy of Science and Humanities,
Minerva Gesellschaft,
Benoziyo Center for High Energy Physics,
Japanese Ministry of Education, Science and Culture (the Monbusho) and a grant under the Monbusho International Science Research Program,
German Israeli Bi-national Science Foundation (GIF),
Bundesministerium für Bildung, Wissenschaft, Forschung und Technologie, Germany,
National Research Council of Canada,
Research Corporation, USA,
Hungarian Foundation for Scientific Research, OTKA T-016660, T023793 and OTKA F-023259.

Appendix

The angular distribution of the decay $\chi_{c2} \to J/\psi\ \gamma \to \ell^+\ell^-\gamma$ can be expressed in terms of the decay helicity amplitudes $A_{|\nu'|}$ [20]

$$W(\theta^*, \theta', \phi') \propto \sum_{\lambda=\pm 2} \sum_{\nu=-2}^{2} \sum_{\nu'=-2}^{2} \sum_{\mu=\pm 1} A^*_{|\nu|}\ A_{|\nu'|}\ d^{J=2}_{\nu\lambda}(\theta^*) d^{J=2}_{\nu'\lambda}(\theta^*)\ \rho^{\sigma\sigma'}(\theta', \phi'), \tag{10}$$

where λ describes the two possible helicities of the χ_{c2} with respect to the $\gamma\gamma$ axis assuming that the χ_{c2} is produced in a helicity ± 2 state. The angles θ^*, θ' and ϕ' are defined in Fig. 1. The indices ν and ν' denote the helicity of the χ_{c2} with respect to the $J/\psi\ \gamma$ axis and the index μ the two possible helicity states of the outgoing photon. The definition of the functions $d^{J=2}_{\nu\lambda}$ can be found in Ref. [8]. The angular distribution of the J/ψ decay is described by the density matrix $\rho^{\sigma\sigma'}$, where $\sigma = \nu - \mu$ and $\sigma' = \nu' - \mu$ are the J/ψ helicities with respect to the $J/\psi\ \gamma$ axis. Explicitly, the angular distribution of the decay $\chi_{c2} \to J/\psi\ \gamma \to \ell^+\ell^-\gamma$ is given by

$$\begin{aligned}
W(\theta^*, \theta', \phi') \propto\ & \frac{1}{8} A_2^2 (1 + \cos^2\theta')(1 + 6\cos^2\theta^* + \cos^4\theta^*) \\
& + A_1^2 (1 - \cos^2\theta')\ (1 - \cos^4\theta^*) \\
& + \frac{3}{4} A_0^2 (1 + \cos^2\theta')\ (1 - 2\cos^2\theta^* + \cos^4\theta^*) \\
& + \frac{1}{2\sqrt{2}} A_2 A_1 (\sin 2\theta' \cos 2\phi')(\sin\theta^* \cos\theta^* (3 - \cos^2\theta^*)) \\
& + \frac{\sqrt{6}}{4} A_2 A_0 (\sin^2\theta' \cos 2\phi')(1 - \cos^4\theta^*) \\
& - \frac{\sqrt{3}}{2}\ A_1 A_0 (\sin 2\phi' \cos 2\phi')(\sin\theta^* \cos\theta^* - \sin\theta^* \cos^3\theta^*).
\end{aligned} \tag{11}$$

The decay amplitudes have been determined to be $A_2 = 0.85 \pm 0.03$, $A_1 = 0.49 \pm 0.03$ and $A_0 = 0.21 \pm 0.05$, based on measurements by E760 [21].

References

[1] E760 Collaboration, T.A. Armstrong et al., Phys. Rev. Lett. 68 (1992) 1468;
E760 Collaboration, T.A. Armstrong et al., Nucl. Phys. B373 (1992) 35.

[2] G.T. Bodwin, E. Braaten and G.P. Lepage, Phys. Rev. D46 (1992) 1914.

[3] G.A. Schuler, F.A. Berends and R. van Gulik, *Meson-photon transition form factors and resonance cross-sections in e^+e^- collisions,* CERN-TH/97-294 (1997) and hep-ph/9710462.

[4] CLEO Collaboration, J. Dominick et al., Phys. Rev. D50 (1994) 4265.

[5] TPC/2γ Collaboration, D.A. Bauer et al., Phys. Lett. B302 (1993) 345.

[6] E760 Collaboration, T.A. Armstrong et al., Phys. Rev. Lett. 70 (1993) 2988.

[7] R704 Collaboration, C. Baglin et al., Phys. Lett. B187 (1987) 191.

[8] R.M. Barnett et al., Review of Particle Physics, Phys. Rev. D54 (1996) 1.

[9] OPAL Collaboration, K. Ahmet et al., Nucl. Instrum. Methods A305 (1991) 275;
P.P. Allport et al., Nucl. Instrum. Methods A346 (1994) 476;
P.P. Allport et al., Nucl. Instrum. Methods A324 (1993) 34;
O. Biebel et al., Nucl. Instrum. Methods A323 (1992) 169;
M. Hauschild et al., Nucl. Instrum. Methods A314 (1992) 74.

[10] B.E. Anderson et al., IEEE Transactions on Nuclear Science 41 (1994) 845.

[11] V.M. Budnev et al., Phys. Rep. 15C (1975) 181.

[12] A. Buijs, W.G.J. Langeveld, M.H. Lehto and D.J. Miller, Comp. Phys. Comm. 79 (1994) 523.

[13] T. Sjöstrand, Comp. Phys. Comm. 82 (1994) 74;
T. Sjöstrand, LUND University Report, LU-TP-95-20 (1995).

[14] J. Allison et al., Nucl. Instrum. Methods A317 (1992) 47.

[15] Z.P. Li, F.E. Close, T. Barnes, Phys. Rev. D43 (1991) 2161.

[16] G.A. Schuler, Comp. Phys. Comm. 108 (1998) 279.

[17] V. Blobel, *Constrained Least Squares and Error Propagation*, to be published, Hamburg (1997).

[18] R.A. Lee, PhD thesis, SLAC-0282, quoted in Ref. [8].

[19] C.N. Yang, Phys. Rev. 77 (1950) 242.

[20] M.G. Olsson and Casimir J. Suchyta III, Phys. Rev. D34 (1986) 2043.

[21] E760 Collaboration, T.A. Armstrong et al., Phys. Rev. D48 (1993) 3037.

Experiment	$\Gamma(\chi_{c2} \to \gamma\gamma)$ [keV]	measured in
CLEO [4]	$1.08 \pm 0.30 \pm 0.26$	$e^+e^- \to e^+e^-\chi_{c2}$
TPC/2γ [5]	$3.4 \pm 1.7 \pm 0.9$	$e^+e^- \to e^+e^-\chi_{c2}$
E760 [6]	$0.321 \pm 0.078 \pm 0.054$	$p\bar{p} \to \chi_{c2} \to \gamma\gamma$
R704 [7]	$2.0 \pm {}^{0.9}_{0.7} \pm 0.3$	$p\bar{p} \to \chi_{c2} \to \gamma\gamma$
average [8]	0.37 ± 0.17	
this measurement	$1.76 \pm 0.47 \pm 0.37 \pm 0.15$	$e^+e^- \to e^+e^-\chi_{c2}$

Table 1: Results on the two-photon width $\Gamma(\chi_{c2} \to \gamma\gamma)$. The first error is statistical, the second error systematic. The CLEO and TPC/2γ results are based on 25.4 ± 6.9 and 6.2 ± 3.0 signal events, respectively. The R704 measurement is updated by using the current world averages for the total width Γ_{tot} and for $BR(\chi_{c2} \to p\overline{p})$ from Ref. [8]. It should be noted that R704 has used an isotropic angular distribution for the decay $\chi_{c2} \to \gamma\gamma$ to calculate their efficiencies.

source	relative error
χ_{c2} decay angular distribution	6%
form factor	5%
energy loss of tracks	4%
minimum cluster energy	11%
background determination	15%
Monte Carlo statistics	2%
quadratic sum	21%

Table 2: Summary of the systematic errors. The errors are added quadratically.

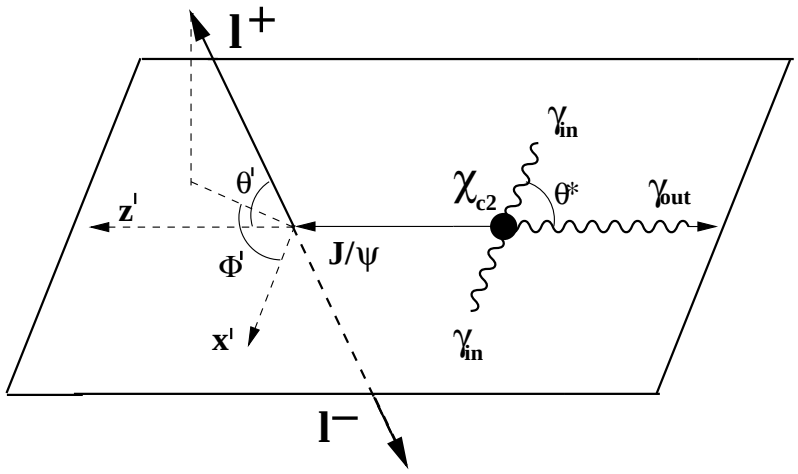

Figure 1: Illustration of the χ_{c2} decay angles: The polar angle θ^* is measured in the χ_{c2} rest frame and is the angle between the χ_{c2} direction of motion in the laboratory system and the direction of the outgoing decay photon ($\gamma_{\rm out}$). The χ_{c2} direction of motion is collinear with the axis of the incoming photons ($\gamma_{\rm in}$). The polar and azimuthal angles of the positive decay lepton ℓ^+, denoted by θ' and ϕ', are measured in the J/ψ rest frame with the z' axis given by the direction opposite to the photon's direction from the χ_{c2} decay, and the x' axis in the plane containing the χ_{c2} direction and the incident photons.

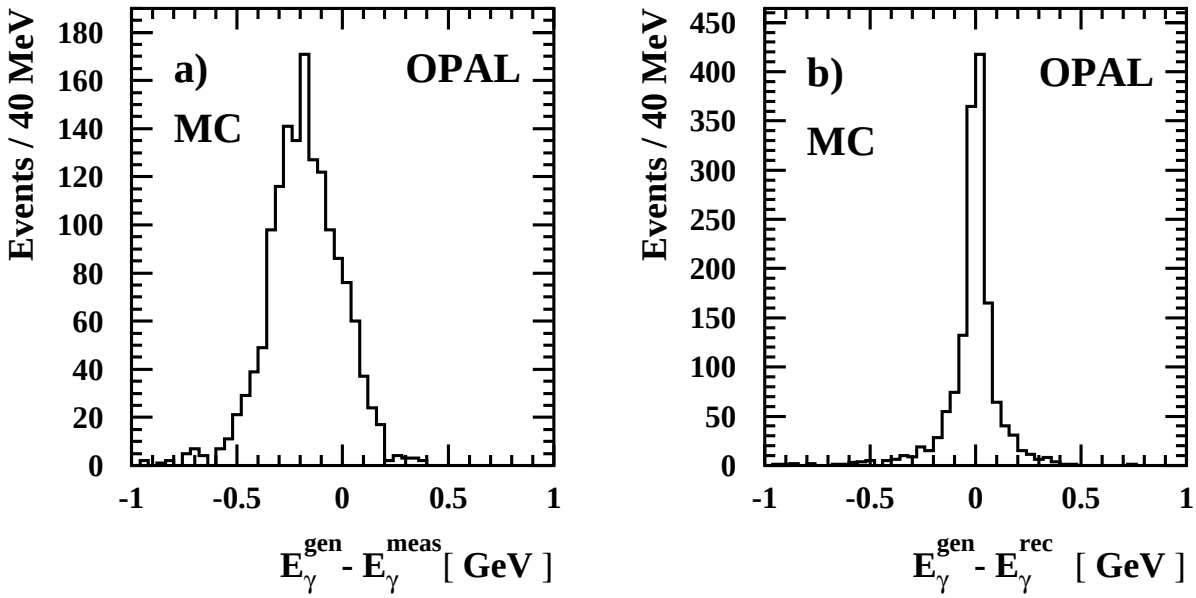

Figure 2: (a) Difference between the generated and the measured photon energy, $E_\gamma^{\rm gen} - E_\gamma^{\rm meas}$, for Monte Carlo (MC) events after applying the cuts described in Section 4. (b) Difference between the generated and the reconstructed photon energy, $E_\gamma^{\rm gen} - E_\gamma^{\rm rec}$, for the same Monte Carlo events.

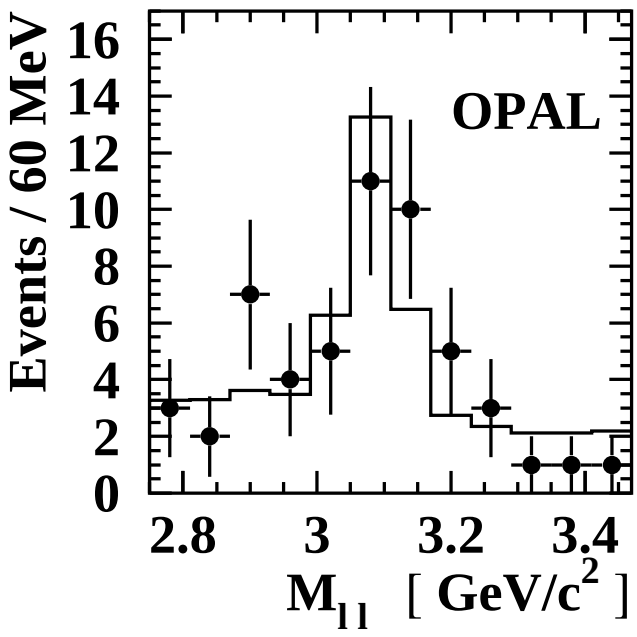

Figure 3: Invariant mass $M_{\ell\ell}$ of the lepton-lepton system after applying the set of cuts as explained in the text and after requiring the invariant mass of the $\ell\ell\gamma$ system to be in the range $3.40 < M_{\ell\ell\gamma} < 3.65$ GeV/c^2 around $M_{\chi_{c2}}$. A peak is visible at the mass of the J/ψ. The dots represent the data, while the histogram shows the normalised Monte Carlo on top of the background determined from data. The Monte Carlo shows a small tail towards lower invariant masses $M_{\ell\ell}$ due to bremsstrahlung and final state radiation of the leptons.

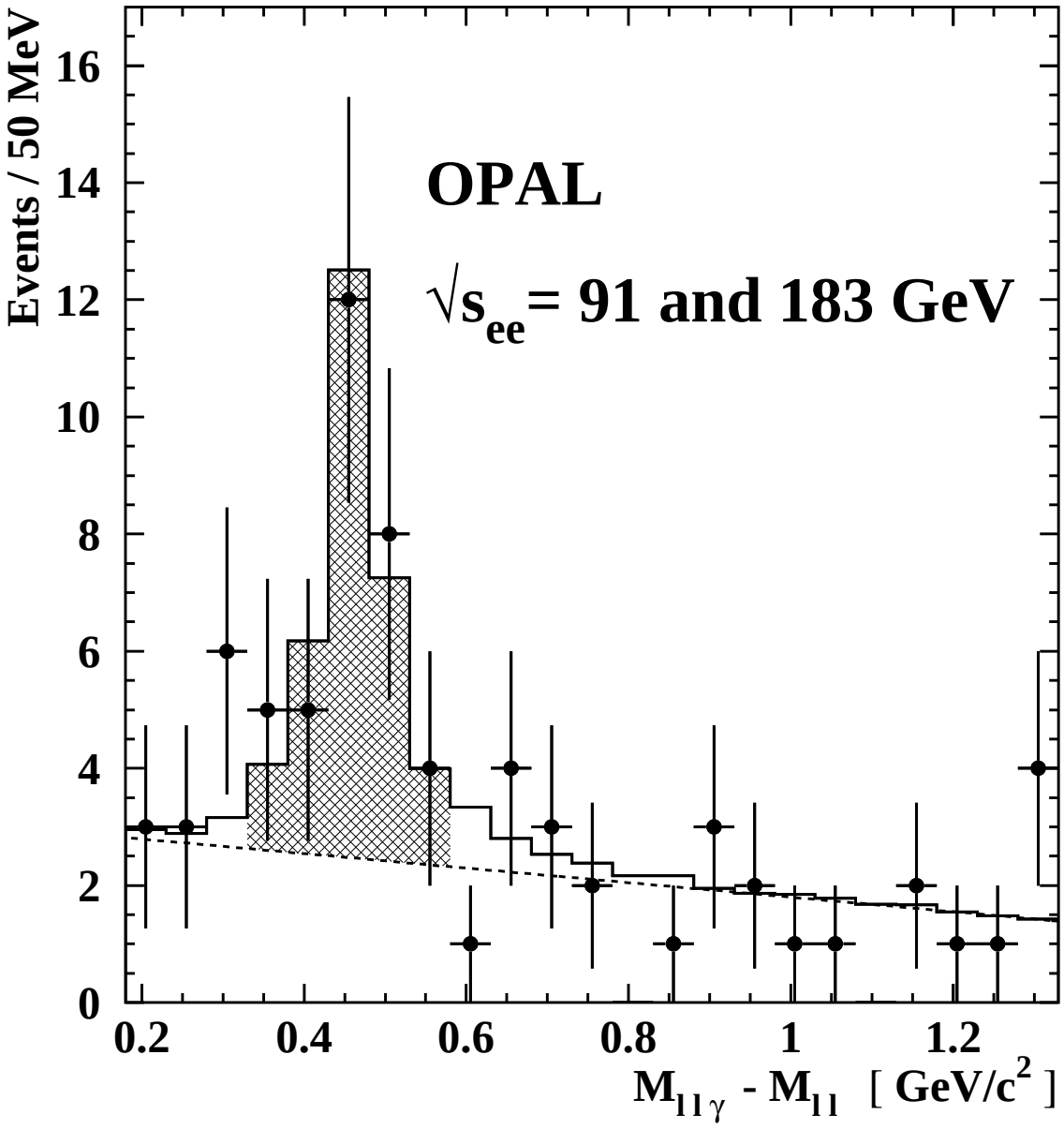

Figure 4: Mass difference between the $\ell\ell\gamma$ and the $\ell\ell$ invariant mass, $M_{\ell\ell\gamma} - M_{\ell\ell}$, after applying the set of cuts explained in the text and after requiring $\mathcal{P}(J/\psi) > 1\%$. A clear peak is visible around $M_{\chi_{c2}} - M_{J/\psi} = 459$ MeV/c^2. The fit of a linear function to the sidebands of the signal is superimposed as dashed line. The open histogram shows the normalised Monte Carlo added to the fitted background. The hatched area represents the invariant mass region between $330 < M_{\ell\ell\gamma} - M_{\ell\ell} < 580$ MeV/c^2.

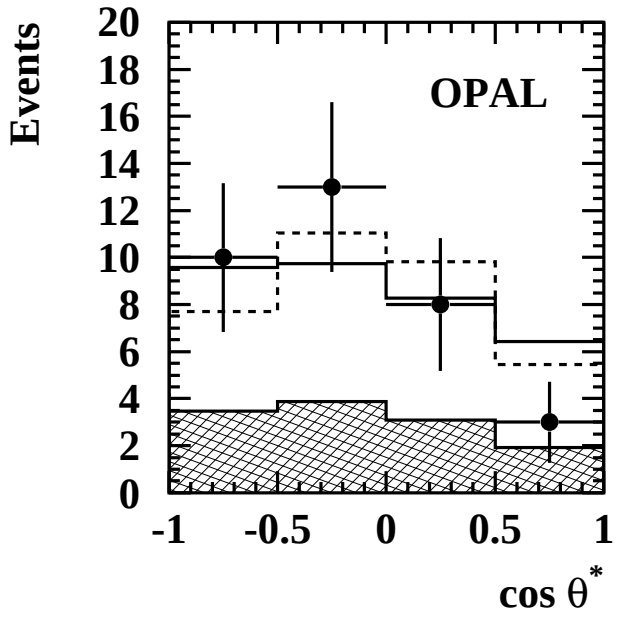

Figure 5: Cosine of the polar angle θ^* of the decay photon in the χ_{c2} rest frame. The dots represent the data with their statistical error, the hatched histogram represents the background taken from the sidebands and then normalised to the number of background events in the signal region, $N^{\rm BG}_{\ell\ell\gamma}$. The full line shows the sum of the normalised background and the signal Monte Carlo with the decay angular distribution as described in Section 3 after normalisation to the number of signal minus background events, $N^{\rm SEL}_{\ell\ell\gamma} - N^{\rm BG}_{\ell\ell\gamma}$. The dashed line is calculated in the same way, but for an isotropic decay angular distribution (spin 0).

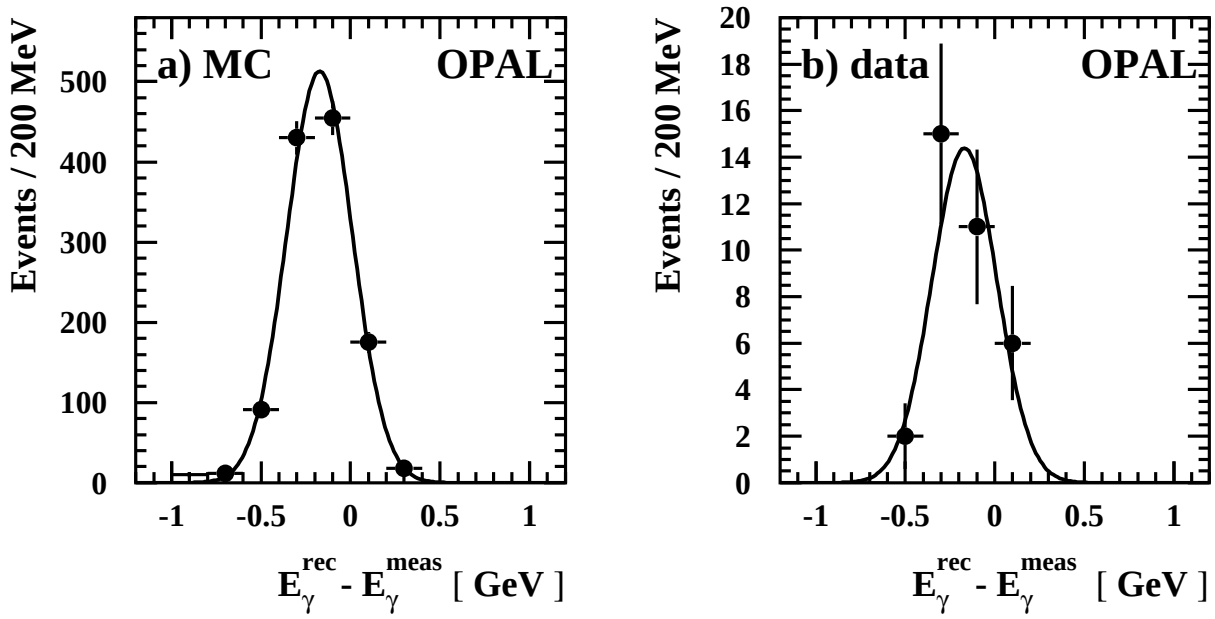

Figure 6: Difference between the reconstructed and the measured photon energy, $E^{\rm rec}_\gamma - E^{\rm meas}_\gamma$, for (a) the Monte Carlo (MC), and (b) the data, after all selection cuts. A Gaussian is fitted to both distributions yielding approximately the same mean and width, but with large errors in case of the data.